International Journal of Mechanical Sciences 104 (2015) 60–74

Contents lists available at ScienceDirect

International Journal of Mechanical Sciences

journal homepage: www.elsevier.com/locate/ijmecsci

A variational Ritz formulation for vibration analysis of thick quadrilateral laminated plates

Rita F. Rango *, Facundo J. Bellomo, Liz G. Nallim

INIQUI – CONICET – Aula CIMNE – Facultad de Ingeniería – Universidad Nacional de Salta, Av. Bolivia 5150, 4400 Salta, Argentina

ARTICLE INFO

Article history:
Received 15 July 2015
Received in revised form
22 September 2015
Accepted 29 September 2015
Available online 22 October 2015

Keywords:
Thick plates
Quadrilateral plates
Ritz method
Free vibration

ABSTRACT

In the present study, a variational Ritz approach for vibration analysis of thick arbitrarily quadrilateral laminated plates, based on the trigonometric shear deformation theory (TSDT) is developed. In this theory, shear stresses are vanished at the top and bottom surfaces of the laminate and shear correction factors are no longer required. A general straight-sided quadrilateral domain is mapped into a square domain in the computational space using a four-node master plate, employing a geometric transformation. The displacement field components are approximated by sets of beam characteristic orthogonal polynomials generated using the Gram–Schmidt procedure. The use of Ritz method allows a high spectral accuracy and faster convergence rates than local methods such as finite element. The algorithm developed is quite general, free of shear locking and can be used to obtain natural frequencies and modal shapes of laminated plates having various material parameters, geometrical planforms, length-to-thickness ratios and any combinations of free, simply supported and clamped edge support conditions.

Through several numerical examples, the capability, efficiency and accuracy of the formulation are demonstrated. Convergence studies and comparison with other existing solutions in the literature suggest that the present algorithm is robust and computationally efficient.

1. Introduction

Due to high strength and stiffness-to-weight ratio of the fiber reinforced composite materials, laminated plates of various shapes composed of these materials have found wide applications as structural members in different engineering fields. Therefore a thorough understanding of the vibration behaviors of composite laminated plates with various geometrical planforms, boundary conditions and length-to-thickness ratios is of great interest for the designers to realize proper and comparatively accurate design of machines and structures. One of the important features of fiber reinforced composite laminates is that they are weak in shear i.e. the value of shear modulus is sufficiently low compared to that of extensional rigidity. Because of this reason the transverse shear deformations are much pronounced for laminated plates than for isotropic ones, so this effect becomes quite significant and it should be considered in the analysis in a proper manner.

The first order shear deformation theories (FSDT) [1,2] which assumes constant transverse shear deformation through the entire thickness of the laminate, violates stress free boundary conditions at the top and bottom surfaces of the plate, and hence shear correction factors need to be involved. Therefore, the accuracy of the FSDT directly depends on this factor which varies with the loading conditions, laminations sequences and boundary conditions as informed by Pai [3]. In order to consider the non-linear transverse shear stress distribution accurately and hence eliminate the requirement of shear correction factor, various higher order shear deformation theories (HSDT) have been proposed. In this kind of plate theories, the transverse shear strain is made non-uniform by taking non-linear through thickness variation of the in-plane displacements. In general, these displacements are approximated by polynomial [4–10] and non-polynomial expressions [11–21]. A clear and precise description of the models, types and classes of theories can be found in the articles by Carrera [22], Reddy and Arciniega [23], and Wanji and Zhen [24].

Along with the development of plate theories, there has been significant development towards the solution methodologies. Particularly, various researchers have addressed the problem of vibration analysis of laminated plates employing HSDT. Liu et al. [25] employed a mesh-free radial basis function method to analyze plates using the third-order shear deformation plate theory. Kant and Swaminathan [26] presented analytical solutions for free vibration of simply supported laminated composite and sandwich plates based on a higher order theory. A Navier type and finite element solutions were proposed by Grover et al. [20] to obtain the free vibration response of laminates, employing an inverse

* Corresponding author. Fax: +54 387 4255351.
E-mail address: ritarango@conicet.gov.ar (R.F. Rango).

http://dx.doi.org/10.1016/j.ijmecsci.2015.09.018
0020-7403/

hyperbolic shear deformation theory. Xiang and Wang [27] employed the trigonometric shear deformation theory (TSDT) and the inverse multiquadric radial basis function (RBF) to predict the free vibration behavior of symmetric laminated plates. RBF have been also applied by Ferreira et al. [28,29] with higher order shear deformation theories for the analysis of laminated composite beams and plates. Thai et al. [21] used an isogeometric analysis for studying laminated composite and sandwich plates within the framework of a new inverse trigonometric theory proposed by the authors. Based on the third order shear deformation theory of Reddy [30], Dai et al. [31] used the moving least-squares method to construct the shape functions for analyzing the static and free vibration behavior of laminated plates.

Carrera [32] developed a powerful formal technique to handle, in a unified manner, an infinite number of equivalent single layer and layer wise axiomatic plate and shell theories with variable-kinematic properties. This technique was employed in several research articles; in particular Dozio and Carrera [33] presented a variable-kinematic Ritz formulation based on two-dimensional higher-order layerwise and equivalent single-layer theories to accurately predict free vibration of skew multi-layered plates.

Recently, an energy-oriented modified Fourier method has been developed to solve vibration problems of generally laminated plates and shells with arbitrary boundary conditions [34–41].

Although there are many references available on free vibration analysis of laminated composite plates, most of them deal with rectangular cross-ply composite plates; while references about the dynamic behavior of general thick quadrilateral laminated composite plates, with any combination of boundary conditions, are rather limited.

Nallim et al. [42] and Nallim and Oller [43] developed a general algorithm for the study the behavior of thin laminated plates based on the Ritz method and a mapping technique to encompass different quadrilateral plate domains. It is important to emphasize that the Ritz method provides upper-bound vibration frequencies [44]. Furthermore, as stated by Dozio and Carrera [33], relying on a global approximation, Ritz method has a high spectral accuracy and converges faster than local methods such as finite element, and it can be quite suitable to provide benchmark references values. For these reasons in this paper a general variational Ritz approach, with sets of beam characteristic Gram–Schmidt orthogonal polynomials as approximating functions, for the dynamical analysis of thick quadrilateral laminated plates is presented. The analysis is based on the trigonometric shear deformation theory [45,46] and the natural coordinates to define a single domain comprehending laminates with different geometries. This variational approach allows investigating the free vibration characteristics of several composite laminated plates of different geometrical planforms, with any combination of boundary conditions and length-to-thickness ratios. The algorithm developed is also very efficient from a computational point of view since a sparse eigenvalue-problem is obtained. Besides, this variational approach can be quite suitable during preliminary design studies and parametric analysis. To demonstrate the validity and efficiency of the proposed formulation, several numerical examples are solved and some of them are verified with results from others authors. New solutions are also presented for future comparison purpose.

2. Formulation

2.1. Description of the model

A quadrilateral laminated plate of total thickness h and arbitrary boundary conditions is considered. The plate has, in general, different side lengths as shown in Fig. 1(a). The laminate consists of N_l layers, which are assumed to be made of orthotropic material, where the fiber angle of the kth layer counted from de surface $z=-h/2$ is β measured from the x axis to the fiber orientation, with all laminae having equal thicknesses, and symmetric lamination of plies is considered. The present study is based on the trigonometric shear deformation theory [45,46]. In this theory the displacement field of a symmetric laminated composite plate can be defined as

$$\begin{aligned}\overline{u}(x,y,z,t) &= u_0 - z\frac{\partial w_0(x,y,t)}{\partial x} + \sin\frac{\pi z}{h}\overline{\phi}_x(x,y,t)\\ \overline{v}(x,y,z,t) &= v_0 - z\frac{\partial w_0(x,y,t)}{\partial y} + \sin\frac{\pi z}{h}\overline{\phi}_y(x,y,t)\\ \overline{w}(x,y,z,t) &= w_0(x,y,t)\end{aligned} \tag{1}$$

where $\overline{u}$ and $\overline{v}$ are the in-plane displacements at any point (x,y,z), u_0 and v_0 denote the in-plane displacement of the point $(x,y,0)$ on the mid-plane, $\overline{w}=w_0$ is the transverse deflection, $\overline{\phi}_x$ and $\overline{\phi}_y$ are the rotations of the normals to the midplane about the y and x axes, respectively. This paper only considers symmetric laminates, therefore we can disregard contributions of u_0, v_0. During free vibration, the displacements are assumed split in the spatial and temporal parts, being them periodic in time:

$$\begin{aligned}w_0(x,y,t) &= w(x,y)\sin(\omega t)\\ \overline{\phi}_x(x,y,t) &= \phi_x(x,y)\sin(\omega t)\\ \overline{\phi}_y(x,y,t) &= \phi_y(x,y)\sin(\omega t)\end{aligned} \tag{2}$$

where ω is the radian natural frequency.

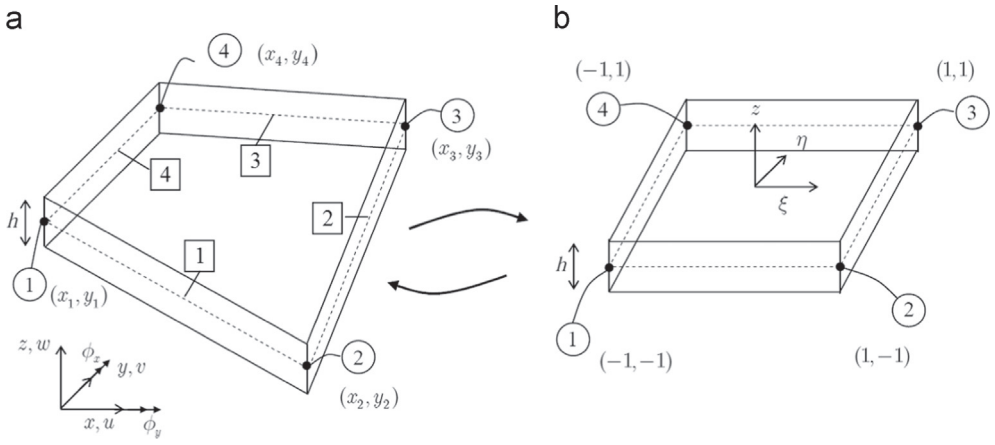

Fig. 1. General quadrilateral thick laminated plate element in: (a) Cartesian coordinates (x,y), and (b) natural coordinates (ξ,η).

The linear strains associated with the displacement fields Eq. (1) are given by:

$$\boldsymbol{\epsilon} = \sin\frac{\pi z}{h}\boldsymbol{\epsilon}_s - z\boldsymbol{\epsilon}_\kappa, \quad \boldsymbol{\gamma} = \frac{\pi}{h}\cos\frac{\pi z}{h}\boldsymbol{\varphi} \tag{3}$$

where:

$$\boldsymbol{\varepsilon} = \left\{ \varepsilon_{xx} \quad \varepsilon_{yy} \quad \gamma_{xy} \right\}^T$$

$$\boldsymbol{\varepsilon}_s = \left\{ \frac{\partial \phi_x}{\partial_x} \quad \frac{\partial \phi_y}{\partial_y} \quad \frac{\partial \phi_x}{\partial_y} \quad \frac{\partial \phi_y}{\partial_x} \right\}^T$$

$$\boldsymbol{\varepsilon}_k = \left\{ \frac{\partial^2 w}{\partial x^2} \quad \frac{\partial^2 w}{\partial y^2} \quad \frac{\partial^2 w}{\partial x \partial y} \right\}$$

$$\boldsymbol{\gamma} = \left\{ \gamma_{yz} \quad \gamma_{xz} \right\}^T \text{ and } \boldsymbol{\varphi} = \left\{ \phi_y \quad \phi_x \right\}^T \tag{4}$$

The stress–strain relationships in the cartesian xyz coordinate system can be written as

$$\begin{Bmatrix} \sigma_{xx} \\ \sigma_{yy} \\ \tau_{xy} \\ \tau_{yz} \\ \tau_{xz} \end{Bmatrix}^{(k)} = \begin{bmatrix} \overline{Q}_{11} & \overline{Q}_{12} & \overline{Q}_{16} & 0 & 0 \\ \overline{Q}_{12} & \overline{Q}_{22} & \overline{Q}_{26} & 0 & 0 \\ \overline{Q}_{16} & \overline{Q}_{26} & \overline{Q}_{66} & 0 & 0 \\ 0 & 0 & 0 & \overline{Q}_{44} & \overline{Q}_{45} \\ 0 & 0 & 0 & \overline{Q}_{45} & \overline{Q}_{55} \end{bmatrix}^{(k)} \begin{Bmatrix} \varepsilon_{xx} \\ \varepsilon_{yy} \\ \gamma_{xy} \\ \gamma_{yz} \\ \gamma_{xz} \end{Bmatrix}^{(k)} \tag{5}$$

where $\overline{Q}_{ij}$ are the mechanical reduced rigidities referred to x, y axes [30].

2.2. Mapping technique

Nallim et al. [42] and Nallim and Oller [43] combined the mapping technique and the Ritz method to derive the eigenfrequency equation for thin laminated plates. This methodology is extended and generalized here to be applied to thick quadrilateral laminated plates.

The actual quadrilateral plate in the Cartesian xy plane (Fig. 1a) is mapped into a square computational domain $-1 \le \xi \le 1$ and $-1 \le \eta \le 1$ in the natural $\xi\eta$ plane (Fig. 1b), using the coordinate transformation:

$$x = \sum_{i=1}^{4} N_i(\xi,\eta)x_i, \quad y = \sum_{i=1}^{4} N_i(\xi,\eta)y_i, \tag{6}$$

where (x_i, y_i), $i = 1, \ldots, 4$ are the corners coordinates of the quadrilateral region R and $N_i(\xi,\eta)$ are the interpolation functions [47] given by:

$$N_i(\xi,\eta) = \frac{1}{4}(1+\eta_i\eta)(1+\xi_i\xi) \tag{7}$$

being (ξ_i, η_i), $i = 1, \ldots, 4$ the corners coordinates of the square computational domain.

Applying the chain rule of differentiation it can be shown that the first and the second derivatives of a function are related by:

$$\begin{bmatrix} \frac{\partial}{\partial x} \\ \frac{\partial}{\partial y} \end{bmatrix} = \mathbf{J}^{-1} \begin{bmatrix} \frac{\partial}{\partial \xi} \\ \frac{\partial}{\partial \eta} \end{bmatrix}, \quad \begin{bmatrix} \frac{\partial^2}{\partial x^2} \\ \frac{\partial^2}{\partial y^2} \\ \frac{\partial^2}{\partial x \partial y} \end{bmatrix} = \frac{1}{|\mathbf{J}|^2}\left[Op^{(1)}\right] \begin{bmatrix} \frac{\partial^2}{\partial \xi^2} \\ \frac{\partial^2}{\partial \eta^2} \\ \frac{\partial^2}{\partial \xi \partial \eta} \end{bmatrix} + \frac{1}{|\mathbf{J}|^3}\left[Op^{(2)}\right] \begin{bmatrix} \frac{\partial}{\partial \xi} \\ \frac{\partial}{\partial \eta} \end{bmatrix} \tag{8}$$

where $\mathbf{J}$ is the Jacobian $\partial(x,y)/\partial(\xi,\eta)$, $|\mathbf{J}|$ is the determinant of this Jacobian matrix and the elements of the matrices $\left[Op^{(1)}\right]$ and $\left[Op^{(2)}\right]$ are given in Appendix A [48,49].

2.3. Approximating functions

The three components of the displacement field are expressed in terms of the natural coordinates system by sets of beam characteristic orthogonal polynomials, i.e: $\left\{p_i^{(w)}(\xi)\right\}$, $\left\{q_j^{(w)}(\eta)\right\}$, $\left\{p_i^{(\phi_x)}(\xi)\right\}$, $\left\{q_j^{(\phi_x)}(\eta)\right\}$, $\left\{p_i^{(\phi_y)}(\xi)\right\}$ and $\left\{q_j^{(\phi_y)}(\eta)\right\}$, as :

$$w(\xi,\eta) = \sum_{i=1}^{m}\sum_{j=1}^{n} c_{ij}^{(w)} p_i^{(w)}(\xi)\, q_j^{(w)}(\eta) = \sum_{i=1}^{m}\sum_{j=1}^{n} c_{ij}^{(w)} N_{ij}^{(w)}(\xi,\eta) = \mathbf{c}^{(w)}\mathbf{N}^{(w)}$$

$$\phi_x(\xi,\eta) = \sum_{i=1}^{m}\sum_{j=1}^{n} c_{ij}^{(\phi_x)} p_i^{(\phi_x)}(\xi)\, q_j^{(\phi_x)}(\eta) = \sum_{i=1}^{m}\sum_{j=1}^{n} c_{ij}^{(\phi_x)} N_{ij}^{(\phi_x)}(\xi,\eta) = \mathbf{c}^{(\phi_x)}\mathbf{N}^{(\phi_x)}$$

$$\phi_y(\xi,\eta) = \sum_{i=1}^{m}\sum_{j=1}^{n} c_{ij}^{(\phi_y)} p_i^{(\phi_y)}(\xi)\, q_j^{(\phi_y)}(\eta) = \sum_{i=1}^{m}\sum_{j=1}^{n} c_{ij}^{(\phi_y)} N_{ij}^{(\phi_y)}(\xi,\eta) = \mathbf{c}^{(\phi_y)}\mathbf{N}^{(\phi_y)} \tag{9}$$

where $c_{ij}^{(w)}$, $c_{ij}^{(\phi_x)}$ and $c_{ij}^{(\phi_y)}$ are the unknown coefficients, and m and n are the numbers of polynomials in each natural co-ordinate.

The procedure for the construction of the orthogonal polynomials has been developed by Bhat [50,51]. The first members of the sets, $p_1^{(\bullet)}(\xi)$ and $q_1^{(\bullet)}(\eta)$ $((\bullet) = w, \phi_x, \phi_y)$ are obtained as the simplest polynomials that satisfy all the geometrical boundary conditions of the plate in their respective ξ and η directions and they are depicted in Appendix B.

The higher members of each set are constructed by employing the Gram–Schmidt orthogonalization procedure. This recurrence procedure ensures the automatic satisfaction of the essential boundary conditions. Besides, the resulting trial functions are linearly independent and form a mathematically complete set in the interval $[-1,+1]$, which ensures very good convergence and numerical stability. Since the Gram–Schmidt orthogonal polynomials satisfy only the geometric boundary conditions they do not over restrain the structure, which is a very important feature in the analysis of general anisotropic plates, because of the bending-twisting coupling [52].

The versatility of this formulation arises from the use of the same sets of orthogonal polynomials for plates of different shapes, which is possible due to the use of natural coordinates.

2.4. Strain and kinetic energies

The strain energy of the laminated plate is given by the following expression:

$$U = \frac{1}{2}\int_R \left\{ \int_{-h/2}^{h/2} \left[\sigma_{xx}^{(k)}\varepsilon_{xx}^{(k)} + \sigma_{yy}^{(k)}\varepsilon_{yy}^{(k)} + \tau_{xy}^{(k)}\gamma_{xy}^{(k)} + \tau_{xz}^{(k)}\gamma_{xz}^{(k)} + \tau_{yz}^{(k)}\gamma_{yz}^{(k)} \right] dz \right\} dR \tag{10}$$

The kinetic energy is given by:

$$T = \frac{1}{2}\int_R \left\{ \int_{-h/2}^{h/2} \rho\left[\dot{u}^2 + \dot{v}^2 + \dot{w}^2\right] dz \right\} dR \tag{11}$$

where the integration is carried out over the entire plate domain R and ρ is the material density.

The integration of the strain energy along the z axis, considering the maximum energy in a cycle, results in the following expression:

$$U_{max} = \frac{1}{2}\int_R \left(\boldsymbol{\epsilon}_s^T\mathbf{A}\boldsymbol{\epsilon}_s + \boldsymbol{\epsilon}_\kappa^T\mathbf{D}\boldsymbol{\epsilon}_\kappa - \boldsymbol{\epsilon}_\kappa^T\mathbf{H}\boldsymbol{\epsilon}_s - \boldsymbol{\epsilon}_s^T\mathbf{H}\boldsymbol{\epsilon}_\kappa + \boldsymbol{\varphi}^T\mathbf{A}^S\boldsymbol{\varphi}\right) dR \tag{12}$$

where:

$$\mathbf{A} = \begin{bmatrix} A_{11} & A_{12} & A_{16} \\ A_{12} & A_{22} & A_{26} \\ A_{16} & A_{26} & A_{66} \end{bmatrix} \quad \mathbf{H} = \begin{bmatrix} H_{11} & H_{12} & H_{16} \\ H_{12} & H_{22} & H_{26} \\ H_{16} & H_{26} & H_{66} \end{bmatrix}$$

$$\mathbf{D} = \begin{bmatrix} D_{11} & D_{12} & D_{16} \\ D_{12} & D_{22} & D_{26} \\ D_{16} & D_{26} & D_{66} \end{bmatrix} \quad \mathbf{A}^S = \begin{bmatrix} A_{44}^S & A_{45}^S \\ A_{45}^S & A_{55}^S \end{bmatrix} \tag{13}$$

being:

$$A_{ij}=\int_{-h/2}^{h/2}\overline{Q}_{ij}^{(k)}\sin^2\left(\frac{\pi z}{h}\right)dz,\quad H_{ij}=\int_{-h/2}^{h/2}\overline{Q}_{ij}^{(k)}z\sin\left(\frac{\pi z}{h}\right)dz,$$

$$D_{ij}=\int_{-h/2}^{h/2}\overline{Q}_{ij}^{(k)}z^2dz,\quad i,j=1,2,6\quad A_{ij}^{s}=\left(\frac{\pi}{h}\right)^2\int_{-h/2}^{h/2}\overline{Q}_{ij}^{(k)}\cos^2\left(\frac{\pi z}{h}\right)dz\quad i,j=4,5 \tag{14}$$

And the maximum kinetic energy in a cycle can be written as:

$$T_{max}=\frac{1}{2}\omega^2\int_R\left\{I_0w^2+I_1\left[\left(\frac{\partial w}{\partial x}\right)^2+\left(\frac{\partial w}{\partial y}\right)^2\right]-2I_2\left[\frac{\partial w}{\partial x}\varphi_x+\frac{\partial w}{\partial y}\varphi_y\right]+I_3\left[(\varphi_x)^2+\left(\varphi_y\right)^2\right]\right\}dR \tag{15}$$

Planform Cartesian Coordinates	1	2	3	4
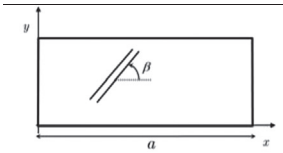 Rectangular	$(0,0)$	$(a,0)$	(a,b)	$(0,b)$
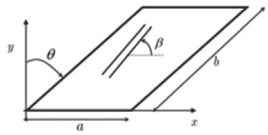 Skew	$(0,0)$	$(a,0)$	$(a+b\sin\theta,b\cos\theta)$	$(b\sin\theta,b\cos\theta)$
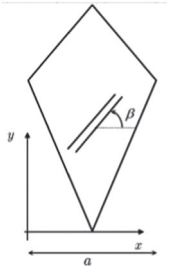 Rhomboidal	$\left(0,\frac{4}{3}a\right)$	$\left(\frac{a}{2},0\right)$	$\left(a,\frac{4}{3}a\right)$	$\left(\frac{a}{2},2a\right)$
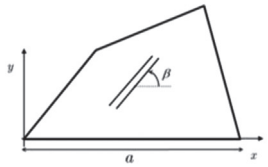 Trapezoidal	$(0,0)$	$(a,0)$	$\left(\frac{5}{6}a,\frac{1}{2}a\right)$	$\left(\frac{1}{3}a,\frac{1}{3}a\right)$

Fig. 2. Plate configurations.

Table 1
Non-dimensional fundamental frequency $\overline{\omega}_1=\omega\left(b^2/h\right)\sqrt{\rho/E_2}$of SSSS square laminated plate (0/90/90/0).

a/h	E_1/E_2	Present					Liu et al. [25]	Reddy [53]
		$m=n$	3	4	5	6	7	
5	3		6.5706	6.5610	6.5601	6.5601	6.5601	6.560	6.557
	10		8.2974	8.2750	8.2737	8.2737	8.2737	8.270	8.272
	20		9.5691	9.5315	9.5302	9.5302	9.5302	9.528	9.526
	30		10.3280	10.2781	10.2769	10.2768	10.2768	10.272	10.279
	40		10.8547	10.7942	10.7931	10.793	10.793	10.773	10.787
10	3		7.2479	7.2446	7.2433	7.2433	7.2433	7.247	7.240
	10		9.8532	9.8437	9.8417	9.8417	9.8417	9.847	9.853
	20		12.2425	12.223	12.2205	12.2204	12.2204	12.225	12.238
	30		13.9002	13.8707	13.8680	13.8680	13.8680	13.892	13.987
	40		15.1546	15.1157	15.113	15.1129	15.1129	15.112	15.143

Table 2
Non-dimensional frequencies $\overline{\omega}_i = \omega_i\left(b^2/\pi^2\right)\sqrt{\rho/D}$ of CCCC rectangular laminated plate (0/90/0).

a/b	a/h	Source	$m=n$	Mode sequence number 1	2	3	4	5	6	7	8
1	10	Present	3	7.920	11.415	15.168	20.202	21.476	28.340	76.504	76.674
			4	7.725	10.574	15.110	16.420	16.851	23.687	24.628	24.989
			5	7.723	10.527	14.966	15.314	16.691	20.171	22.653	23.572
			6	7.673	10.491	14.962	15.262	16.684	20.121	21.147	23.571
			7	7.672	10.459	14.899	15.254	16.612	20.070	21.142	23.567
		Shi et al. [54]		7.451	10.451	13.993	15.534	15.896	19.698	21.618	21.773
		Liew [55]		7.411	10.393	13.913	15.429	15.806	19.572	21.489	21.620
	20	Present	3	11.351	14.725	23.405	24.448	27.859	34.267	79.560	80.335
			4	11.158	14.182	21.356	24.278	26.010	32.680	36.756	39.804
			5	11.157	14.164	20.383	23.986	25.714	29.842	31.216	39.332
			6	11.084	14.101	20.325	23.984	25.710	29.115	29.818	36.625
			7	11.084	14.086	20.305	23.797	25.523	29.112	29.634	36.493
		Shi et al. [54]		11.015	14.152	20.691	23.323	25.142	29.532	29.777	36.665
		Liew [55]		10.953	14.028	20.388	23.196	24.978	29.237	29.369	36.266
	100	Present	3	14.468	17.529	25.195	38.610	40.314	44.739	80.535	81.606
			4	14.450	17.405	25.087	37.925	38.517	39.538	44.126	53.584
			5	14.450	17.404	24.298	37.880	38.202	39.491	43.532	53.304
			6	14.442	17.395	24.291	35.332	37.870	39.481	43.523	51.162
			7	14.442	17.394	24.264	35.331	37.827	39.437	43.464	50.329
		Shi et al. [54]		14.666	17.614	24.511	35.532	39.157	40.768	44.786	50.297
		Liew [55]		14.583	17.762	25.004	36.644	38.073	39.802	44.082	51.725
2	10	Present	3	4.207	6.916	8.443	10.580	19.765	20.212	20.897	21.800
			4	4.151	6.846	8.285	10.005	10.485	13.003	14.202	15.627
			5	4.150	6.779	8.232	9.911	10.352	12.684	13.808	14.509
			6	4.128	6.772	8.223	9.907	10.324	12.662	13.776	14.278
			7	4.128	6.729	8.182	9.842	10.322	12.634	13.769	14.270
		Shi et al. [54]		4.164	6.652	8.401	9.950	10.023	12.513	13.743	14.221
		Liew [55]		4.141	6.617	8.354	9.895	9.967	12.443	13.659	14.120
	20	Present	3	4.811	9.088	9.989	12.947	20.447	20.492	22.252	22.652
			4	4.787	8.983	9.818	12.605	15.370	17.905	18.216	20.122
			5	4.786	8.936	9.797	12.546	14.982	17.511	17.526	19.341
			6	4.776	8.933	9.790	12.544	14.953	17.495	17.498	19.328
			7	0.775	8.894	9.771	12.496	14.945	17.476	17.479	19.287
		Shi et al. [54]		4.838	8.910	9.982	12.647	14.824	17.467	17.996	19.744
		Liew [55]		4.779	8.840	9.847	12.511	14.703	17.300	17.673	19.429
	100	Present	3	5.092	10.616	10.724	14.468	20.583	20.717	23.065	23.130
			4	5.091	10.449	10.551	14.241	20.254	20.604	22.697	22.972
			5	5.091	10.446	10.550	14.237	19.321	19.628	21.896	22.121
			6	5.090	10.444	10.547	14.233	19.319	19.628	21.893	22.119
			7	5.090	10.441	10.546	14.230	19.288	19.594	21.865	22.088
		Shi et al. [54]		5.250	10.697	11.012	14.726	19.697	20.420	22.445	22.933
		Liew [55]		5.105	10.527	10.583	14.324	19.567	19.701	22.148	22.237

Table 3
Non-dimensional fundamental frequency $\overline{\omega}_1 = \omega(a^2/h)\sqrt{\rho/E_2}$ of CCCC square laminated plate.

	Source	$m=n$	a/h 4	10	20	100
0/90/90/0	Present	3	12.250	23.834	33.375	41.333
		4	12.019	23.229	32.854	41.290
		5	11.971	23.218	32.853	41.289
		6	11.929	23.031	32.645	41.269
		7	11.920	23.027	32.644	41.269
	Akhras and Li [56]		11.865	23.033	32.622	41.265
45/-45/-45/45	Present	3	12.052	22.916	31.009	36.831
		4	11.693	22.156	30.235	36.630
		5	11.604	22.036	30.102	36.576
		6	11.533	21.832	29.900	36.540
		7	11.517	21.798	29.855	36.528
	Akhras and Li [56]		11.510	21.883	29.935	36.575

where:

$$\left[I_0,\quad I_1,\quad I_2,\quad I_3\right] = \int_{-h/2}^{h/2} \rho\left[1,\quad z^2,\quad z\ \text{sen}\frac{\pi z}{h},\quad \text{sen}^2\frac{\pi z}{h}\right] dz \tag{16}$$

Substituting Eq. (9) into Eqs. (12) and (15) and applying the mapping technique Eq. (8), the following expressions for the maximum strain and kinetic energies are obtained:

$$U_{max} = \frac{1}{2}\int_{-1}^{1}\int_{-1}^{1}\left\{\mathbf{c}^T\left[\mathbf{B}^{(1)}\mathbf{A}\left(\mathbf{B}^{(1)}\right)^T\right]\mathbf{c} + \mathbf{c}^T\left[\mathbf{B}^{(2)}\mathbf{D}\left(\mathbf{B}^{(2)}\right)^T\right]\mathbf{c} - \mathbf{c}^T\left[\mathbf{B}^{(2)}\mathbf{H}\left(\mathbf{B}^{(1)}\right)^T\right]\mathbf{c} - \mathbf{c}^T\left[\mathbf{B}^{(1)}\mathbf{H}\left(\mathbf{B}^{(2)}\right)^T\right]\mathbf{c} + \mathbf{c}^T\left[\mathbf{B}^{(3)}\mathbf{A}^S\left(\mathbf{B}^{(3)}\right)^T\right]\mathbf{c}\right\}|\mathbf{J}|d\xi d\eta \tag{17}$$

$$T_{max} = \frac{1}{2}\omega^2\int_{-1}^{1}\int_{-1}^{1}\left\{\mathbf{c}^T\left[\mathbf{B}^{(4)}\mathbf{B}^{(5)}\mathbf{B}^{(6)}\right]\mathbf{c} + \mathbf{c}^T\left[\mathbf{B}^{(7)}\mathbf{B}^{(8)}\right]\mathbf{c}\right\}|\mathbf{J}|d\xi d\eta \tag{18}$$

where:

$$\mathbf{c} = \left[\mathbf{c}^{(w)}\quad \mathbf{c}^{(\phi_x)}\quad \mathbf{c}^{(\phi_y)}\right]^T$$

Table 4
Non-dimensional frequencies $\overline{\omega}_i = \omega_i\left(b^2/\pi^2\right)\sqrt{\rho/D}$ of FCFC skew isotropic plate with: $E=1,\ \ \nu=0.3,\ \ a/h=10,\ \ a/b=1$.

θ	Source	Mode sequence number					
		1	2	3	4	5	6
0°	Present	2.0984	2.4509	3.9325	5.3797	5.8376	7.0561
	Eftekhari and Jafari [57]	2.0901	2.4337	3.9052	5.3385	5.7801	6.9365
15°	Present	2.1997	2.5259	4.0398	5.6269	6.0628	6.9335
	Eftekhari and Jafari [57]	2.1896	2.5062	4.0105	5.5779	5.9924	6.8407
30°	Present	2.5249	2.6583	5.0086	5.4531	6.7987	7.6272
	Eftekhari and Jafari [57]	2.5251	2.7572	4.3988	6.2596	6.6924	7.2222
45°	Present	3.2925	3.3986	5.3997	7.3480	8.3902	9.2013
	Eftekhari and Jafari [57]	3.2419	3.3262	5.3561	7.1976	8.1346	8.9959
60°	Present	4.8930	4.9770	7.8620	9.3310	11.3860	14.0630
	Eftekhari and Jafari [57]	4.7094	4.8359	7.7189	9.0729	11.1286	13.4549

Table 5
Non-dimensional frequencies $\overline{\omega}_i = \omega_i\left(a^2/h\right)\sqrt{\rho/E_2}$ of SSFC skew plates.

a/h	$0/\beta/0$	$\overline{\omega}_1$	$\overline{\omega}_2$	$\overline{\omega}_3$	$\overline{\omega}_4$	$\overline{\omega}_5$	$\overline{\omega}_6$
5	0/15/0	9.3866	11.3351	16.3124	21.1590	22.7583	23.2144
	0/30/0	9.0144	11.1024	16.5222	20.3284	21.9619	23.6700
	0/45/0	8.6399	10.9678	16.9746	19.4783	21.3529	24.0582
	0/60/0	8.3616	10.9998	17.4644	18.8594	21.1737	24.2481
	0/75/0	8.2288	11.1703	17.6945	18.6113	21.4790	24.2992
	0/90/0	8.2517	11.3751	17.6600	18.7098	21.9921	24.2063
10	0/15/0	14.7806	16.9938	23.7421	34.9235	35.8769	37.5158
	0/30/0	14.3137	16.6509	23.9126	34.1682	36.0530	36.2588
	0/45/0	13.8299	16.3343	24.4430	32.8265	34.9519	37.2007
	0/60/0	13.4634	16.2107	25.2663	31.7761	34.2084	37.8462
	0/75/0	13.2788	16.3541	25.9672	31.2278	34.2607	37.9939
	0/90/0	13.2936	16.6737	26.1869	31.2445	34.9554	37.8776
100	0/15/0	22.3889	25.2931	33.9551	51.6847	71.5977	74.3067
	0/30/0	22.2470	25.3270	34.4857	53.0965	71.0722	74.0314
	0/45/0	22.1601	25.2801	35.1586	55.5219	70.7728	73.7073
	0/60/0	22.1205	25.2809	36.1384	58.7454	70.6249	73.4664
	0/75/0	22.1187	25.5301	37.3595	61.5371	70.5739	73.6189
	0/90/0	22.1617	26.0225	38.3276	62.5227	70.6800	74.2971
1000	0/15/0	22.5426	25.4711	34.1897	52.0671	72.8538	75.5957
	0/30/0	22.4150	25.5232	34.7422	53.5044	72.4397	75.4542
	0/45/0	22.3469	25.4939	35.4280	55.9516	72.2908	75.2853
	0/60/0	22.3240	25.5076	36.4147	59.2112	72.2791	75.1726
	0/75/0	22.3326	25.7670	37.6529	62.0777	72.3103	75.4012
	0/90/0	22.3781	26.2686	38.6512	63.1426	72.4314	76.0992

$$\mathbf{B}^{(1)} = \begin{bmatrix} 0 & 0 & 0 \\ \mathbf{A1}^{(x)} & 0 & \mathbf{A2}^{(x)} \\ 0 & \mathbf{A2}^{(y)} & \mathbf{A1}^{(y)} \end{bmatrix}; \quad \mathbf{B}^{(2)} = \begin{bmatrix} \mathbf{A3} & \mathbf{A4} & 2\mathbf{A5} \\ 0 & 0 & 0 \\ 0 & 0 & 0 \end{bmatrix};$$

$$\mathbf{B}^{(3)} = \begin{bmatrix} 0 & 0 \\ 0 & \mathbf{N}^{(\phi_x)} \\ \mathbf{N}^{(\phi_y)} & 0 \end{bmatrix}; \quad \mathbf{B}^{(4)} = \begin{bmatrix} \left[\left(\mathbf{A1}'\right)^2 + \left(\mathbf{A2}'\right)\right]^2 & \mathbf{A1}' & \mathbf{A2}' \\ 0 & 0 & 0 \\ 0 & 0 & 0 \end{bmatrix};$$

Table 6
Non-dimensional frequencies $\overline{\omega}_i = \omega_i\left(a^2/h\right)\sqrt{\rho/E_2}$ of CFSF skew plates.

a/h	$0/\beta/0$	$\overline{\omega}_1$	$\overline{\omega}_2$	$\overline{\omega}_3$	$\overline{\omega}_4$	$\overline{\omega}_5$	$\overline{\omega}_6$
5	0/15/0	4.2537	5.7687	11.4068	12.5250	18.6181	19.3528
	0/30/0	4.5015	6.0352	11.9852	13.1748	18.1817	20.0871
	0/45/0	4.8715	6.2885	12.8223	13.8391	17.7587	20.5320
	0/60/0	5.2191	6.4914	13.6189	14.2988	17.5968	20.5957
	0/75/0	5.3584	6.6146	13.9105	14.5378	17.7147	20.3463
	0/90/0	5.2349	6.6205	13.6255	14.5314	17.9464	19.8729
10	0/15/0	5.0925	7.2070	15.4287	17.1541	27.2040	28.3297
	0/30/0	5.3546	7.5505	16.1056	18.0263	26.8090	29.5797
	0/45/0	5.8305	7.8771	17.3518	19.0732	26.3763	30.7295
	0/60/0	6.3548	8.1554	18.7705	19.9809	26.1789	31.1270
	0/75/0	6.6311	8.3604	19.5390	20.4839	26.3700	30.9236
	0/90/0	6.5172	8.4048	19.2558	20.4803	26.7808	30.2643
100	0/15/0	5.5831	8.3547	18.7878	21.3539	35.9527	38.0398
	0/30/0	5.8279	8.7662	19.4018	22.3715	36.0538	39.8660
	0/45/0	6.3519	9.1311	20.9712	23.7724	36.0607	42.3608
	0/60/0	7.0044	9.4412	23.1568	25.2274	36.1562	43.7446
	0/75/0	7.4336	9.7532	24.7802	26.2412	36.6729	43.9112
	0/90/0	7.4034	9.9233	24.8644	26.4158	37.4618	43.2600
1000	0/15/0	5.5907	8.3798	18.8435	21.4354	36.1125	38.2273
	0/30/0	5.8346	8.7926	19.4533	22.4533	36.2281	40.0616
	0/45/0	6.3588	9.1576	21.0255	23.8575	36.2459	42.5853
	0/60/0	7.0132	9.4671	23.2249	25.3212	36.3484	43.9950
	0/75/0	7.4460	9.7825	24.8711	26.3491	36.8768	44.1764
	0/90/0	7.4198	9.9600	24.9786	26.5349	37.6848	43.5427

Table 7
Non-dimensional frequencies $\overline{\omega}_i = \omega_i\left(a^2/h\right)\sqrt{\rho/E_2}$ of CSSC skew plates.

a/h	$0/\beta/0$	$\overline{\omega}_1$	$\overline{\omega}_2$	$\overline{\omega}_3$	$\overline{\omega}_4$	$\overline{\omega}_5$	$\overline{\omega}_6$
5	0/15/0	10.8833	15.4844	21.9291	22.4415	25.6205	28.6103
	0/30/0	10.6180	15.6589	21.5247	22.5572	25.2052	29.0898
	0/45/0	10.4422	16.0702	20.8127	23.1090	25.4682	29.5364
	0/60/0	10.4268	16.5697	20.4759	23.3694	26.3769	29.8698
	0/75/0	10.5492	16.9199	20.5992	23.4485	27.3017	29.9438
	0/90/0	10.7281	17.0031	21.0382	23.3712	27.8185	29.7476
10	0/15/0	16.4352	22.8578	33.5244	36.9277	41.3508	45.3926
	0/30/0	16.0629	22.9852	34.3446	35.5838	40.3953	46.1894
	0/45/0	15.7540	23.4874	34.2519	35.6547	40.0312	46.9763
	0/60/0	15.6458	24.3007	33.4476	36.5791	40.9242	47.6006
	0/75/0	15.7636	25.0510	33.3405	36.8886	42.5111	47.8174
	0/90/0	16.0193	25.3716	33.8706	36.8157	43.6107	47.5374
100	0/15/0	24.3509	32.7631	49.6731	72.9732	74.6501	79.5924
	0/30/0	24.3224	33.1917	50.9166	72.7939	76.7439	79.5010
	0/45/0	24.3342	33.9381	53.3128	72.5508	79.4007	81.1917
	0/60/0	24.4299	35.0998	56.6499	72.4043	79.6799	86.2562
	0/75/0	24.6769	36.4480	59.6214	72.5183	80.7896	89.2235
	0/90/0	25.0419	37.4052	60.7584	73.0105	82.5286	89.7283
1000	0/15/0	24.5157	32.9784	50.0337	74.0791	75.5455	80.9632
	0/30/0	24.5034	33.4254	51.2956	74.1666	77.5213	81.0033
	0/45/0	24.5331	34.1857	53.7143	74.0937	81.0354	82.0555
	0/60/0	24.6427	35.3581	57.0927	74.0804	81.4198	87.3640
	0/75/0	24.8992	36.7235	60.1353	74.2729	82.5772	90.5994
	0/90/0	25.2702	37.7044	61.3399	74.7819	84.3367	91.1851

$$\mathbf{B}^{(5)} = \begin{bmatrix} I_1 & 0 & 0 \\ 0 & -2I_2 & 0 \\ 0 & 0 & -2I_2 \end{bmatrix}; \quad \mathbf{B}^{(6)} = \begin{bmatrix} 1 & 0 & 0 \\ 0 & \mathbf{N}^{(\phi_x)} & 0 \\ 0 & 0 & \mathbf{N}^{(\phi_y)} \end{bmatrix};$$

Table 8
Non-dimensional frequencies $\overline{\omega}_i = \omega_i(a^2/h)\sqrt{\rho/E_2}$ of SFFC skew plates.

a/h	$0/\beta/0$	$\overline{\omega}_1$	$\overline{\omega}_2$	$\overline{\omega}_3$	$\overline{\omega}_4$	$\overline{\omega}_5$	$\overline{\omega}_6$
5	0/15/0	3.8275	6.2052	12.4405	13.2703	15.6884	18.5078
	0/30/0	3.7321	6.3831	12.7025	13.0784	15.4541	18.9249
	0/45/0	3.6195	6.6416	12.2954	13.5405	15.5113	19.2962
	0/60/0	3.5280	6.8733	11.9710	13.6173	16.0436	19.4913
	0/75/0	3.4819	6.9190	11.8339	13.3972	16.5718	19.4175
	0/90/0	3.4872	6.7468	11.8706	13.0681	16.7451	19.1465
10	0/15/0	4.7987	7.7806	16.7116	20.3906	23.4724	27.2871
	0/30/0	4.7427	8.0069	17.4629	19.7601	23.0299	28.0385
	0/45/0	4.6610	8.2881	18.5381	19.1250	22.6430	28.6668
	0/60/0	4.5883	8.5402	18.5939	19.3475	22.8213	28.9612
	0/75/0	4.5539	8.6281	18.3840	19.2530	23.5947	28.9114
	0/90/0	4.5670	8.4942	18.4355	18.7139	24.2051	28.5162
100	0/15/0	5.3987	9.1232	20.3908	32.0260	36.3874	38.2166
	0/30/0	5.3919	9.4422	21.2486	31.8301	36.4438	40.0309
	0/45/0	5.3526	9.7365	22.6928	31.6879	36.3127	42.4166
	0/60/0	5.3111	9.9670	24.3056	31.6123	36.2855	43.6534
	0/75/0	5.3004	10.1073	25.2259	31.6064	36.8386	43.6611
	0/90/0	5.3310	10.1008	24.9903	31.6749	37.8312	43.0096
1000	0/15/0	5.4075	9.1516	20.4648	32.2875	36.7056	38.4415
	0/30/0	5.4015	9.4724	21.3208	32.1153	36.7927	40.2707
	0/45/0	5.3625	9.7661	22.7658	32.0037	36.6888	42.7143
	0/60/0	5.3214	9.9958	24.3883	31.9554	36.6804	44.0206
	0/75/0	5.3111	10.1395	25.3331	31.9665	37.2487	44.0503
	0/90/0	5.3423	10.1415	25.1243	32.0398	38.2649	43.4046

Table 9
Non-dimensional frequencies $\overline{\omega}_i = \omega_i(a^2/h)\sqrt{\rho/E_2}$ of SSFC rhomboidal plates.

a/h	$0/\beta/0$	$\overline{\omega}_1$	$\overline{\omega}_2$	$\overline{\omega}_3$	$\overline{\omega}_4$	$\overline{\omega}_5$	$\overline{\omega}_6$
5	0/15/0	9.5299	13.0444	17.1786	20.7300	22.5293	26.7810
	0/30/0	9.1987	12.8262	17.0242	20.3507	22.0180	26.3624
	0/45/0	8.9403	12.6693	17.0030	19.9404	21.8377	25.8908
	0/60/0	8.8218	12.6157	17.1244	19.6315	21.9901	25.4726
	0/75/0	8.8612	12.6713	17.3008	19.5814	22.2921	25.2274
	0/90/0	9.0484	12.8008	17.4081	19.8694	22.5233	25.2478
10	0/15/0	14.1846	18.8542	25.5402	31.8039	35.4584	41.8776
	0/30/0	13.8399	18.6398	25.3854	31.4916	34.5755	41.3329
	0/45/0	13.5469	18.4924	25.3978	31.2652	33.9277	40.9693
	0/60/0	13.4055	18.4825	25.6089	31.0934	33.8381	40.5121
	0/75/0	13.4638	18.6192	25.9127	31.1239	34.1828	40.1305
	0/90/0	13.7168	18.8463	26.1293	31.5789	34.5323	40.1957
100	0/15/0	21.3764	25.9204	37.0866	50.8747	67.5809	76.8987
	0/30/0	21.3285	26.0094	37.4601	51.3953	67.7986	76.9079
	0/45/0	21.3368	26.1803	38.0330	52.3359	68.2563	77.3252
	0/60/0	21.3873	26.5114	38.7759	53.6161	68.6252	78.2968
	0/75/0	21.5111	27.0054	39.5563	54.9229	68.8280	79.5486
	0/90/0	21.7213	27.5345	40.1363	55.7841	69.0390	80.4841
1000	0/15/0	21.7390	26.1731	37.4115	51.7551	69.1075	78.7233
	0/30/0	21.7161	26.2780	37.8145	52.3535	69.4687	78.8621
	0/45/0	21.7541	26.4667	38.4248	53.3910	70.1146	79.4037
	0/60/0	21.8251	26.8203	39.2051	54.7671	70.6712	80.4235
	0/75/0	21.9516	27.3434	40.0167	56.1405	71.0018	81.6428
	0/90/0	22.1472	27.9031	40.6140	57.0075	71.2431	82.5239

Table 10
Non-dimensional frequencies $\overline{\omega}_i = \omega_i(a^2/h)\sqrt{\rho/E_2}$ of CFSF rhomboidal plates.

a/h	$0/\beta/0$	$\overline{\omega}_1$	$\overline{\omega}_2$	$\overline{\omega}_3$	$\overline{\omega}_4$	$\overline{\omega}_5$	$\overline{\omega}_6$
5	0/15/0	6.9074	7.8897	11.7889	15.0946	18.5117	20.0398
	0/30/0	7.1332	8.0377	11.9262	15.3802	18.7938	20.1097
	0/45/0	7.1872	8.2390	12.0711	15.6498	18.8710	20.2556
	0/60/0	7.0543	8.3182	12.1731	15.8349	18.6478	20.3599
	0/75/0	6.7909	8.1790	12.1357	15.8523	18.2072	20.2183
	0/90/0	6.4999	7.8912	11.9263	15.6860	17.6658	19.8913
10	0/15/0	9.0434	10.7231	16.6520	21.1902	26.9767	30.3238
	0/30/0	9.5220	10.8366	16.9136	21.7260	27.5434	30.2835
	0/45/0	9.8472	11.0063	17.2107	22.3026	28.2116	30.1386
	0/60/0	9.7983	11.1245	17.4232	22.7243	28.4448	29.9872
	0/75/0	9.4695	11.0110	17.3830	22.8060	27.9578	29.7833
	0/90/0	9.0605	10.7060	17.0335	22.4879	27.1617	29.4017
100	0/15/0	12.2152	14.1946	22.9090	28.9233	40.0102	52.4956
	0/30/0	12.8748	14.4575	23.5996	30.0839	41.1937	53.3654
	0/45/0	13.4650	14.7814	24.3942	31.6368	42.9196	54.2187
	0/60/0	13.6501	15.0379	24.9445	32.9300	44.5449	54.6281
	0/75/0	13.4576	15.0272	24.9744	33.4160	45.3485	54.4651
	0/90/0	13.0468	14.7749	24.4412	32.8881	45.0464	53.9675
1000	0/15/0	12.4645	14.4589	23.1837	29.1817	40.6369	53.9353
	0/30/0	13.1399	14.7350	23.9009	30.3631	41.8983	54.9334
	0/45/0	13.7504	15.0706	24.7224	31.9579	43.7223	55.9458
	0/60/0	13.9539	15.3309	25.2837	33.2952	45.4310	56.4833
	0/75/0	13.7702	15.3220	25.3057	33.8000	46.2902	56.3835
	0/90/0	13.3553	15.0746	24.7565	33.2614	45.9986	55.8720

Table 11
Non-dimensional frequencies $\overline{\omega}_i = \omega_i(a^2/h)\sqrt{\rho/E_2}$ of CSSC rhomboidal plates.

a/h	$0/\beta/0$	$\overline{\omega}_1$	$\overline{\omega}_2$	$\overline{\omega}_3$	$\overline{\omega}_4$	$\overline{\omega}_5$	$\overline{\omega}_6$
5	0/15/0	12.4587	16.6782	21.1160	25.8731	26.3324	32.3050
	0/30/0	12.1623	16.4644	20.9368	25.1100	26.1239	31.5527
	0/45/0	11.8540	16.2875	20.8517	24.3525	26.0663	30.8414
	0/60/0	11.6054	16.1831	20.8981	23.7129	26.1836	30.2854
	0/75/0	11.4569	16.1391	21.0175	23.2773	26.3620	29.9219
	0/90/0	11.4276	16.1319	21.0727	23.1515	26.4404	29.8003
10	0/15/0	19.4027	25.9862	32.9358	40.9818	42.6745	51.6869
	0/30/0	19.0091	25.6674	32.6195	40.5382	41.4645	51.0789
	0/45/0	18.5704	25.3612	32.4122	40.0311	40.3734	50.1429
	0/60/0	18.2047	25.1323	32.3833	38.8848	40.3895	48.9791
	0/75/0	17.9833	24.9957	32.4716	38.0830	40.6177	48.1344
	0/90/0	17.9397	24.9618	32.5276	37.8480	40.7539	47.8176
100	0/15/0	31.4952	43.6346	58.5176	79.0688	90.8430	109.1567
	0/30/0	31.5231	44.0420	59.1370	79.7068	90.6106	109.7518
	0/45/0	31.5679	44.5708	60.0001	80.6558	90.2256	110.6850
	0/60/0	31.6388	45.0568	60.8840	81.6963	89.7861	111.7095
	0/75/0	31.7250	45.3926	61.5554	82.5539	89.4400	112.5211
	0/90/0	31.7958	45.5378	61.8192	82.9092	89.3321	112.8061
1000	0/15/0	32.7025	44.3200	59.3574	80.6952	94.4023	112.0327
	0/30/0	32.7620	44.7579	60.0632	81.4640	94.3652	112.8849
	0/45/0	32.8327	45.3442	61.0249	82.5649	94.2250	114.1233
	0/60/0	32.9230	45.8983	61.9907	83.7404	94.0167	115.4078
	0/75/0	33.0206	46.2935	62.7116	84.6989	93.8185	116.3809
	0/90/0	33.0895	46.4726	62.9865	85.1146	93.7178	116.7119

Table 12
Non-dimensional frequencies $\overline{\omega}_i = \omega_i (a^2/h)\sqrt{\rho/E_2}$ of SFFC rhomboidal plates.

a/h	$0/\beta/0$	$\overline{\omega}_1$	$\overline{\omega}_2$	$\overline{\omega}_3$	$\overline{\omega}_4$	$\overline{\omega}_5$	$\overline{\omega}_6$
5	0/15/0	2.3271	5.2267	8.2991	11.7036	15.0885	16.5453
	0/30/0	2.4284	5.3637	8.5344	12.0218	15.3727	16.2274
	0/45/0	2.5234	5.5301	8.8585	12.4766	15.4179	16.3675
	0/60/0	2.5564	5.6471	9.1573	12.9418	15.1875	16.9385
	0/75/0	2.5112	5.6756	9.3048	13.2603	15.0273	17.4234
	0/90/0	2.4312	5.6452	9.2656	13.3275	14.9691	17.6688
10	0/15/0	2.6628	6.4744	10.8731	16.2579	22.1464	24.5024
	0/30/0	2.7979	6.7161	11.2694	16.8064	22.6750	24.1287
	0/45/0	2.9268	6.9692	11.7492	17.5247	22.9963	24.1982
	0/60/0	2.9716	7.1149	12.1306	18.2069	22.7559	24.9610
	0/75/0	2.9106	7.1143	12.2652	18.6091	22.5010	25.6477
	0/90/0	2.8024	7.0239	12.1542	18.5659	22.3777	25.9539
100	0/15/0	2.9746	7.4639	13.0080	20.7980	30.7204	35.7760
	0/30/0	3.1391	7.7993	13.5889	21.7758	31.9684	35.7838
	0/45/0	3.3005	8.1327	14.2520	22.9235	33.5076	35.8338
	0/60/0	3.3608	8.3088	14.7340	23.8517	34.5215	36.1794
	0/75/0	3.2919	8.2924	14.8770	24.2364	34.5516	36.9464
	0/90/0	3.1607	8.1726	14.7349	24.0257	34.1210	37.5077
1000	0/15/0	2.9916	7.4936	13.0613	20.9277	31.0292	36.0867
	0/30/0	3.1574	7.8310	13.6469	21.9264	32.3049	36.1162
	0/45/0	3.3200	8.1655	14.3138	23.0919	33.8759	36.1906
	0/60/0	3.3809	8.3411	14.7976	24.0225	34.9107	36.5569
	0/75/0	3.3118	8.3234	14.9409	24.3956	34.9455	37.3418
	0/90/0	3.1800	8.2036	14.8002	24.1769	34.5083	37.9222

$$\mathbf{B}^{(7)} = \begin{bmatrix} I_0 & 0 & 0 \\ 0 & I_3 & 0 \\ 0 & 0 & I_3 \end{bmatrix}; \quad \mathbf{B}^{(8)} = \begin{bmatrix} \mathbf{N}^{(w)} & 0 & 0 \\ 0 & \mathbf{N}^{(\phi_x)} & 0 \\ 0 & 0 & \mathbf{N}^{(\phi_y)} \end{bmatrix}; \tag{19}$$

with:

$$\mathbf{A}1^{(x)} = \frac{J_{22}}{|\mathbf{J}|}\frac{\partial \mathbf{N}^{(\phi_x)}}{\partial \xi} - \frac{J_{12}}{|\mathbf{J}|}\frac{\partial \mathbf{N}^{(\phi_x)}}{\partial \eta}, \quad \mathbf{A}2^{(x)} = -\frac{J_{21}}{|\mathbf{J}|}\frac{\partial \mathbf{N}^{(\phi_x)}}{\partial \xi} + \frac{J_{11}}{|\mathbf{J}|}\frac{\partial \mathbf{N}^{(\phi_x)}}{\partial \eta}$$

$$\mathbf{A}1^{(y)} = \frac{J_{22}}{|\mathbf{J}|}\frac{\partial \mathbf{N}^{(\phi_y)}}{\partial \xi} - \frac{J_{12}}{|\mathbf{J}|}\frac{\partial \mathbf{N}^{(\phi_y)}}{\partial \eta}, \quad \mathbf{A}2^{(y)} = -\frac{J_{21}}{|\mathbf{J}|}\frac{\partial \mathbf{N}^{(\phi_y)}}{\partial \xi} + \frac{J_{11}}{|\mathbf{J}|}\frac{\partial \mathbf{N}^{(\phi_y)}}{\partial \eta}$$

$$\mathbf{A}3 = a_1'\frac{\partial^2 \mathbf{N}^{(w)}}{\partial \xi^2} + a_2'\frac{\partial^2 \mathbf{N}^{(w)}}{\partial \eta^2}, \quad \mathbf{A}4 = b_1'\frac{\partial^2 \mathbf{N}^{(w)}}{\partial \xi^2} + b_2'\frac{\partial^2 \mathbf{N}^{(w)}}{\partial \eta^2}$$

$$\mathbf{A}5 = -c_1'\frac{\partial^2 \mathbf{N}^{(w)}}{\partial \xi^2} - c_2'\frac{\partial^2 \mathbf{N}^{(w)}}{\partial \eta^2} \tag{20}$$

$$\mathbf{A}1' = \frac{\partial \mathbf{N}^{(w)}}{\partial x} = \frac{J_{22}}{|J|}\frac{\partial \mathbf{N}^{(w)}}{\partial \xi} - \frac{J_{12}}{|J|}\frac{\partial \mathbf{N}^{(w)}}{\partial \eta}$$

$$\mathbf{A}2' = \frac{\partial \mathbf{N}^{(w)}}{\partial y} = -\frac{J_{21}}{|J|}\frac{\partial \mathbf{N}^{(w)}}{\partial \xi} + \frac{J_{11}}{|J|}\frac{\partial \mathbf{N}^{(w)}}{\partial \eta} \tag{21}$$

3. Application of the Ritz method

The Ritz method is applied to determine analytical approximate solutions for thick laminated plates of different shapes. In the previous section the expressions for the maximum strain Eq. (17) and kinetic Eq. (18) energies have been derived, and the resulting total energy functional for free vibration can be written as:

$$F_d = U_{max} - T_{max} \tag{22}$$

For the dynamical analysis the Ritz procedure requires the minimization of the energy functional Eq. (22) with respect to each of the $c_{ij}^{(w)}$, $c_{ij}^{(\phi_x)}$ and $c_{ij}^{(\phi_y)}$ coefficients, i.e.:

$$\frac{\partial F_d}{\partial c_{ij}^{(w)}} = 0, \quad \frac{\partial F_d}{\partial c_{ij}^{(\phi_x)}} = 0, \quad \frac{\partial F_d}{\partial c_{ij}^{(\phi_y)}} = 0 \quad (i,j = 1,\ldots,m,n) \tag{23}$$

Then from Eq. (23), the following standard generalized eigenvalue problem is obtained:

$$(\mathbf{K} - \omega^2 \mathbf{M})\mathbf{c} = \mathbf{0} \tag{24}$$

where the stiffness matrix $\mathbf{K}$ and the mass matrix $\mathbf{M}$ are respectively given by:

$$\mathbf{K} = \int_{-1}^{1}\int_{-1}^{1} \left[\mathbf{B}^{(1)}\mathbf{A}\left(\mathbf{B}^{(1)}\right)^T + \mathbf{B}^{(2)}\mathbf{D}\left(\mathbf{B}^{(2)}\right)^T - \mathbf{B}^{(2)}\mathbf{H}\left(\mathbf{B}^{(1)}\right)^T - \mathbf{B}^{(1)}\mathbf{H}\left(\mathbf{B}^{(2)}\right)^T + \mathbf{B}^{(3)}\mathbf{A}^S\left(\mathbf{B}^{(3)}\right)^T\right]|\mathbf{J}|d\xi d\eta \tag{25}$$

$$\mathbf{M} = \int_{-1}^{1}\int_{-1}^{1} \left[\mathbf{B}^{(4)}\mathbf{B}^{(5)}\mathbf{B}^{(6)} + \mathbf{B}^{(7)}\mathbf{B}^{(8)}\right]|\mathbf{J}|d\xi d\eta \tag{26}$$

4. Verification and numerical applications

4.1. Generalities

The variational algorithm developed was implemented on a computer code and several plates with different shapes, material properties, thickness ratios and boundary conditions have been analyzed, determining their natural frequencies and modal shapes.

The use of the trigonometric shear deformation theory allows the analysis of thick laminates without the need of a shear correction factor. Also, the numerical determination of eigenfrequencies (global responses) of laminates of any length-to-thickness ratio is possible because this formulation does not exhibit any shear looking issues.

In order to establish the accuracy and applicability of the described approach, numerical results were computed for a number of plate problems for which comparison values are available in the literature. These examples are presented to demonstrate the accuracy and efficiency of the proposed method, and to produce results which may be regarded as benchmark solutions for other academic research workers and design engineers.

Four-letter compact symbolic notation is used for describing simply supported (S), clamped (C) and free (F) boundary conditions, numbered in a counterclock-wise direction beginning from edge (1) (Fig. 1). The material properties used in the following sections are:

$$M1: E_1/E_2 = 40, \quad G_{12} = G_{13} = 0.6E_2, \quad G_{23} = 0.5E_2, \quad \nu_{12} = 0.25$$

$$M2: E_1/E_2 = 25, \quad G_{12} = G_{13} = 0.5E_2, \quad G_{23} = 0.2E_2, \quad \nu_{12} = 0.25$$

The plate geometries used in this article are detailed in Fig. 2.

4.2. Convergence and comparison of eigenvalues

To test the validity of the proposed formulation two convergence analysis and two validation examples considering different laminates and boundary conditions were performed. The convergence is studied by gradually increasing the number of polynomials used in each natural coordinate for each variable w, ϕ_x, ϕ_y.

Results of the convergence study of non-dimensional fundamental frequencies $\overline{\omega}_1$ are presented in Table 1 for simply supported (0/90/90/0) cross-ply laminates considering different a/h ratios. Material properties of $M1$ are used in this section, but with different values for E_1/E_2. The results are in good agreement with those published by Liu et al. [25] and Reddy [53].

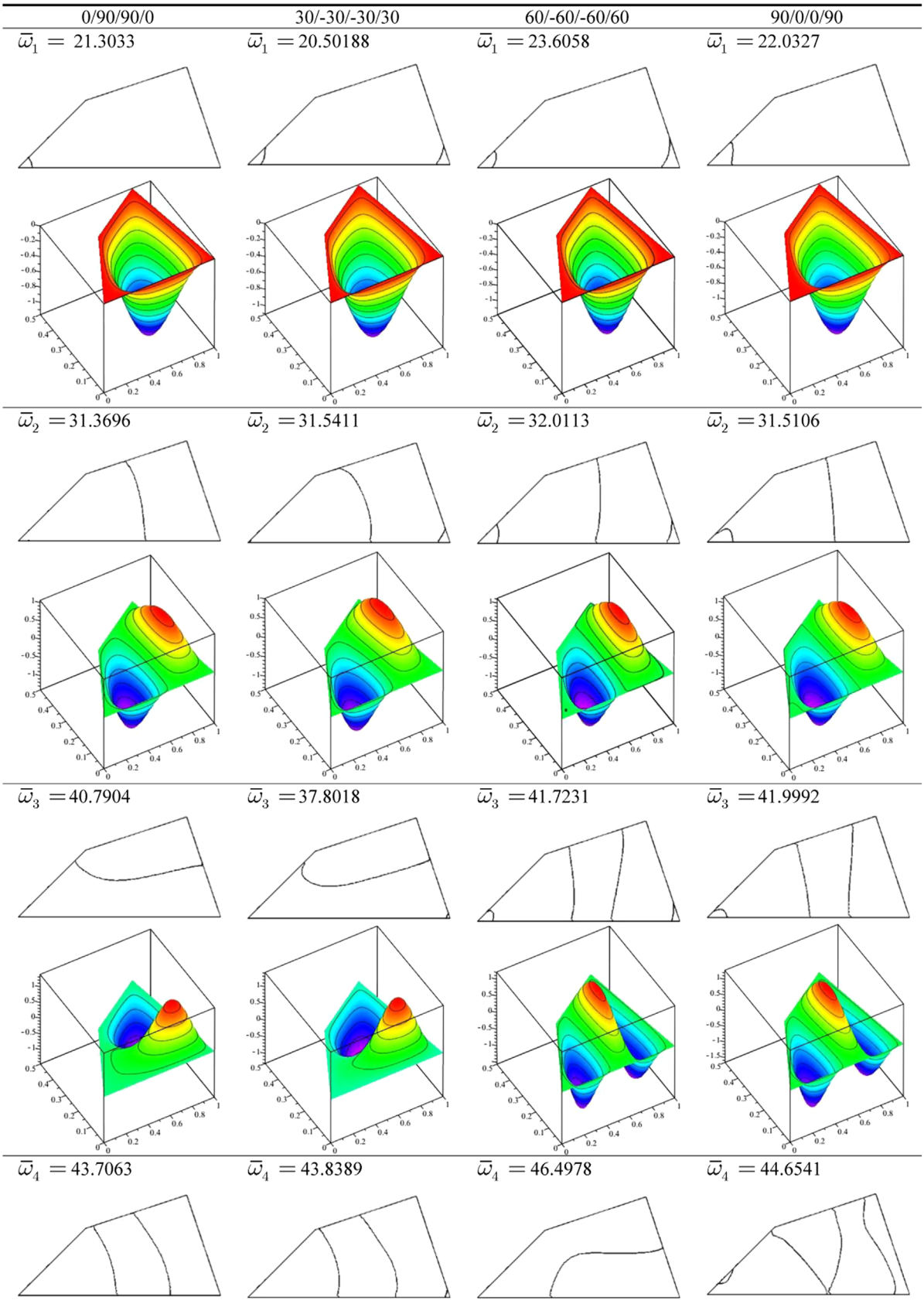

Fig. 3. First six modal shapes of thick trapezoidal laminates with SSSS boundary conditions.

Table 2 presents a convergence study and a comparison with Shi et al. [54] and Liew [55], of the first eight non-dimensional frequencies $\overline{\omega}_i = \omega_i \left(b^2/\pi^2\right)\sqrt{\rho/D}$, where $D = E_2 h^3/12(1-\nu_{12}\nu_{21})$, for a symmetric cross-ply fully clamped rectangular laminated plate with material $M1$, with various thickness ratios a/h and two different aspect ratios a/b. As can be seen in this case at least 7 polynomials are needed to obtain convergence for the

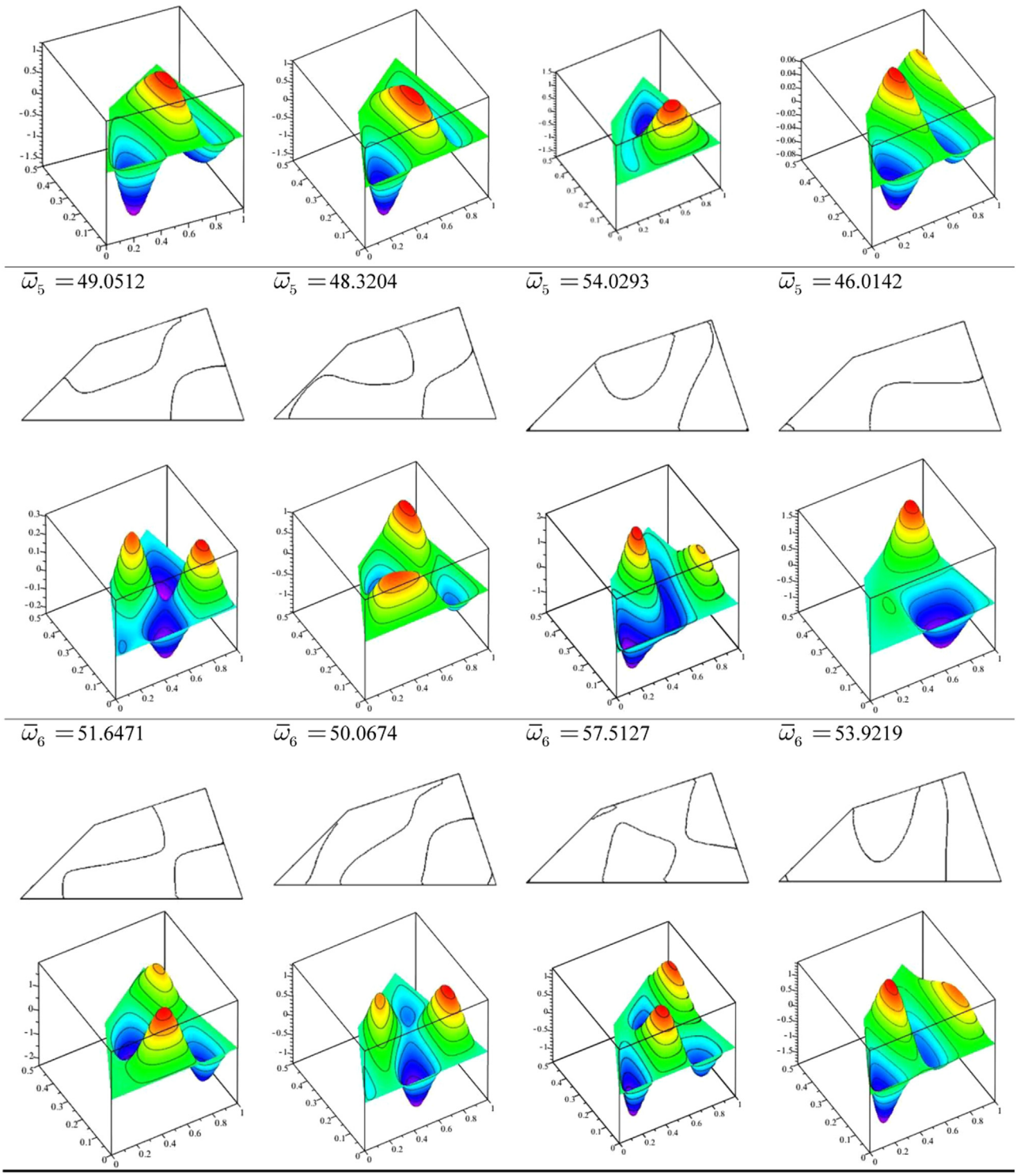

Fig. 3. (*continued*)

higher frequencies while the fundamental frequency value convergence is attained with 5 polynomials in each natural coordinate. Therefore, it was decided to use $m, n = 7$ to generate the results with sufficient accuracy from an engineering viewpoint.

The proposed formulation was also validated by comparing with the results published by Akhras and Li [56] who use a spline finite strip method with Reddy's Higher Order Shear Deformation Theory, regarding the fundamental frequency for square cross-ply and angle-ply laminates in Table 3. Material $M1$ is also used in this case. The obtained results agree very well for both laminates with those of Akhras and Li [56].

To test the validity of the model for non-rectangular plates several cases regarding isotropic skew plates are compared with Eftekhari and Jafari [57] who use a modified mixed Ritz-differential quadrature formulation. The skew plate configuration is detailed in Fig. 2. The results are shown in Table 4. A good agreement was obtained in all cases.

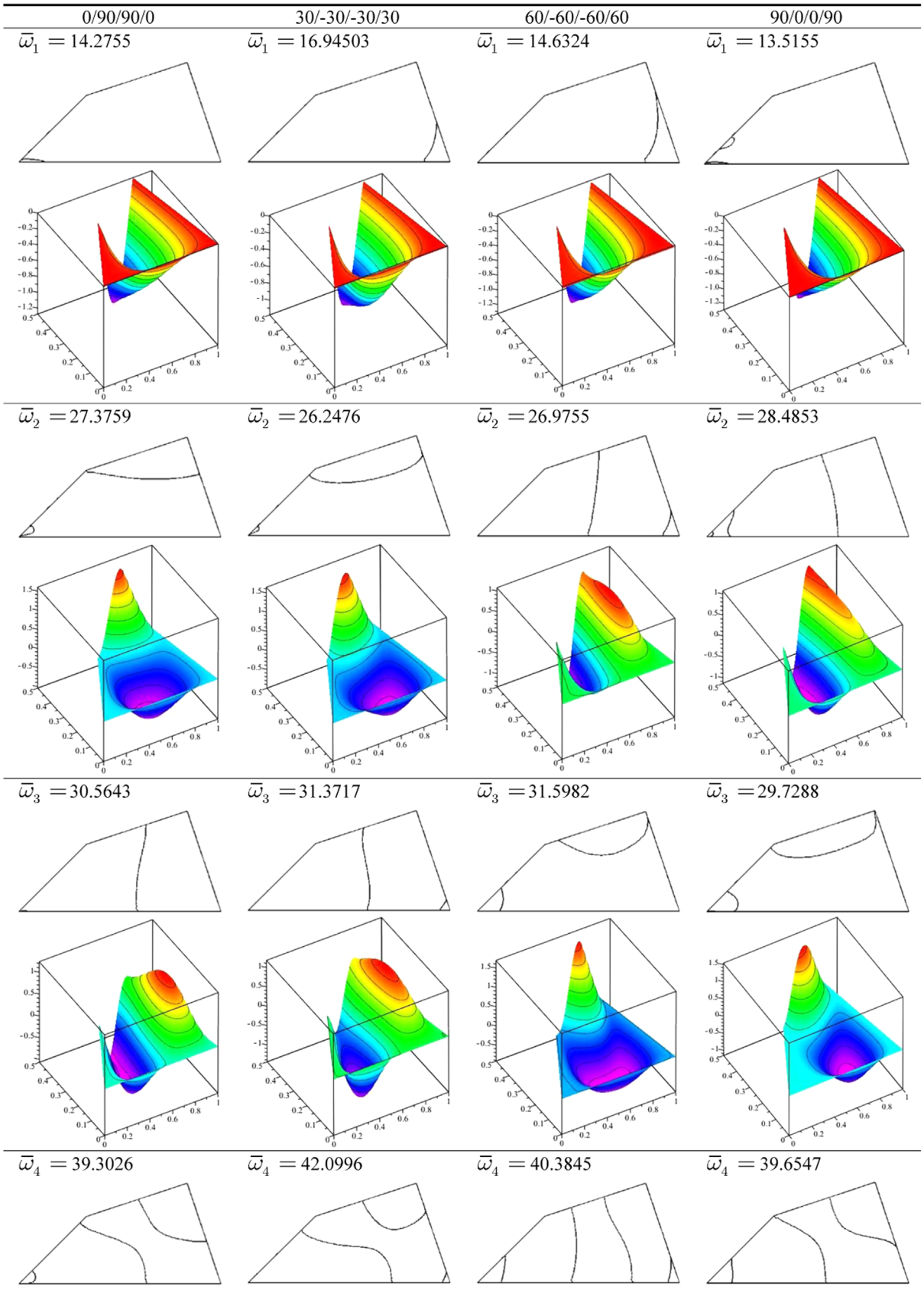

Fig. 4. First six modal shapes of thick trapezoidal laminates with SSFC boundary conditions.

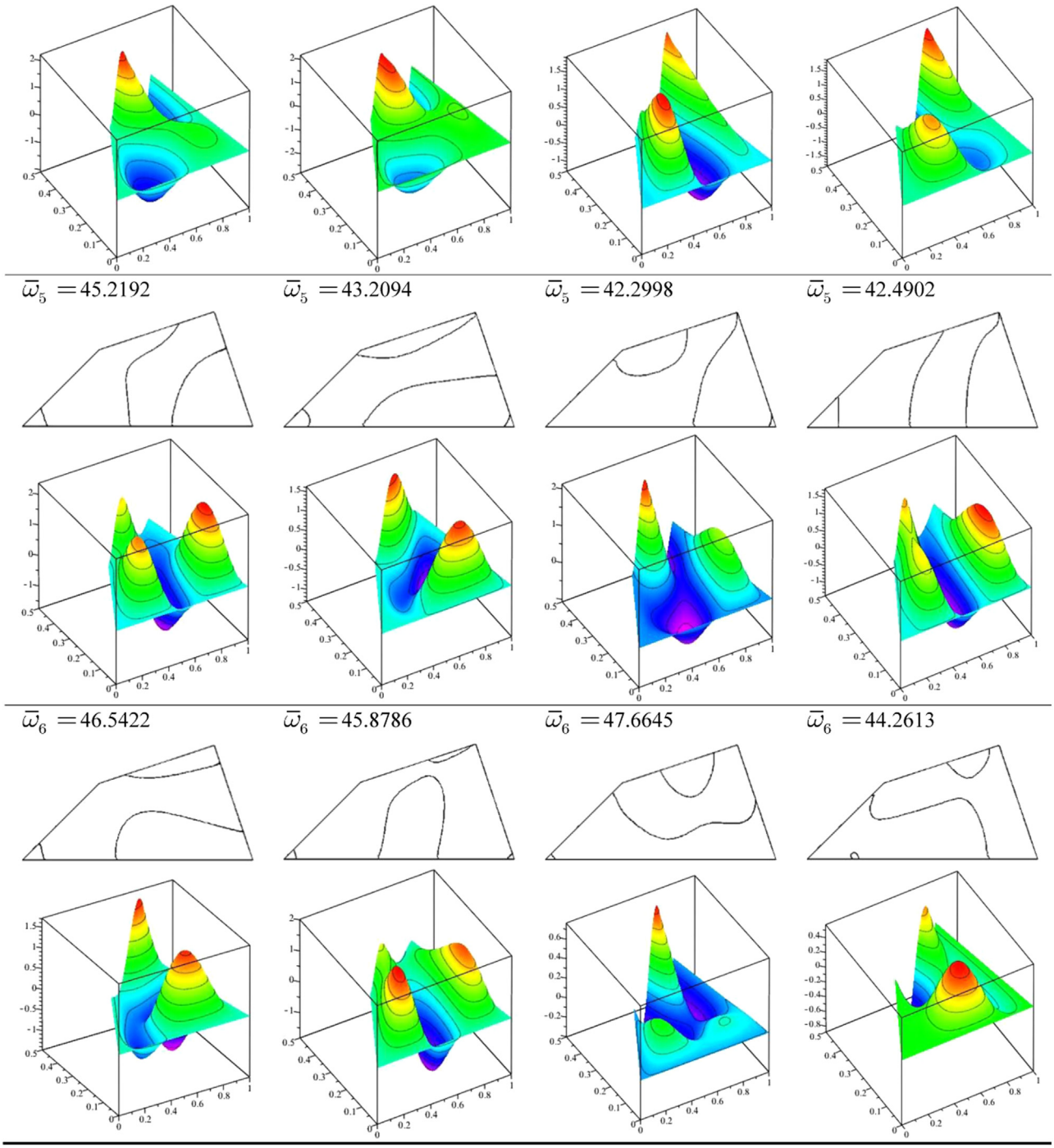

Fig. 4. (*continued*)

4.3. Application to general quadrilateral thick plates

The proposed formulation can be used to determine accurately the free vibration behavior of different quadrilateral laminates. To illustrate this fact, Tables 5–8 show the first six non-dimensional natural frequencies of thick skew plates with skew angle $\theta = 30^{\circ}$, and Tables 9–12 show the first six non-dimensional natural frequencies of thick rhomboidal plates, for different stacking sequences and different boundary conditions. The *M*2 material properties are used in this section.

The lower fundamental frequencies for the SSFC and SFFC skew plates with $a/h = 5, 10, 100, 1000$ occur for $\beta = 75^{\circ}$ with the single exception of the SSFC case with $a/h = 1000$ for which the minimum occurs for $\beta = 60^{\circ}$. The maximum values are obtained for $\beta = 15^{\circ}$ in all cases. It can be observed that the influence of the fiber orientation in the frequency values is more important for lower a/h ratios. For CFSF skew plates the dynamical behavior is quite different, the lowest fundamental frequency values are obtained for $\beta = 15^{\circ}$ and the maximum values for $\beta = 75^{\circ}$. In this case the maximum and minimum values are obtained for the same fiber orientation, independently of the length-to-thickness ratio. The fundamental frequency values for skew plates with CSSC boundary conditions are lowest for $\beta = 60^{\circ}$ with $a/h = 5, 10$ and $\beta = 30^{\circ}$ with $a/h = 100, 1000$. The maximum values are obtained for $\beta = 15^{\circ}$ with $a/h = 5, 10$ and $\beta = 90^{\circ}$ with $a/h = 100, 1000$. However the fiber orientation effect is less noticeable in this case for all length-to-thickness ratios.

The lower fundamental frequencies for the SSFC rhomboidal plates with $a/h=5,10$ occurs for $\beta=60^\circ$ and with $a/h=100,1000$ for $\beta=30^\circ$. The maximum values are obtained for $\beta=15^\circ$ with $a/h=5,10$ and for $\beta=90^\circ$ with $a/h=100,1000$. For SFFC rhomboidal plates the lowest fundamental frequency values are obtained for $\beta=15^\circ$ and the maximum values for $\beta=60^\circ$. In this case the maximum and minimum values are obtained for the same fiber orientation, independently of the length-to-thickness ratio. The fundamental frequency values for rhomboidal plates with CSSC boundary conditions are lowest for $\beta=90^\circ$ with $a/h=5,10$ and $\beta=15^\circ$ with $a/h=100,1000$. The maximum values are obtained for $\beta=15^\circ$ with $a/h=5,10$ and $\beta=90^\circ$ with $a/h=100,1000$. The fundamental frequency values for CFSF rhomboidal plates are lowest for $\beta=90^\circ$ with $a/h=5$ and $\beta=15^\circ$ with $a/h=10,100,1000$. The maximum values are obtained for $\beta=45^\circ$ with $a/h=5,10$ and $\beta=60^\circ$ with $a/h=100,1000$.

Finally, results are presented of the developed approach applied to study the dynamical behavior of thick trapezoidal laminates. Material *M*2 is used and thickness ratio is $a/h=5$. Four different stacking sequences are analyzed and the first six natural frequencies of free vibration were determined $\overline{\omega}_i=\omega_i(a^2/h)\sqrt{\rho/E_2}$. Results for simply supported SSSS thick laminates are plotted in Fig. 3.

The first two modal shapes are very similar for the four laminates. The effect of the different stacking sequences can be observed from mode 3 and on, where the behavior of 0/90/90/0 and 30/-30/-30/30 laminates is similar but clearly different of the behavior exhibited by 60/-60/-60/60 and 90/0/0/90 laminates.

Results for SSFC boundary conditions are presented in Fig. 4.

5. Conclusions

A Ritz approach has been developed for the study of the dynamical behavior of symmetrically laminated thick plates. The proposed method is based on the trigonometric plate theory and uses natural coordinates to express the geometry of different laminates in a simple form. The approximation function are sets of orthogonal polynomials generated using the Gram–Schmidt procedure resulting in a general algorithm that allows the analysis of a variety of geometrical shapes, material properties and combinations of classical boundary conditions.

This paper formulation could be useful for structural design engineers as it can provide benchmark values to assess the accuracy of the eigen frequencies of polygonal thick plates with different thickness and general boundary conditions, usually calculated using FEM packages. The present algorithm also includes the effects of shear deformation and all rotary inertias.

Numerical applications include rectangular, skew, and general quadrilateral thick laminates, for which natural frequencies and modal shapes of free vibration have been obtained. In all cases analyzed for validation purposes, a very close agreement was found. Also the capability to consider any arbitrary quadrilateral shape results in a very versatile and efficient analysis tool for the determination of natural frequencies and modal shapes in an important number of plate problems of interest in design works.

Aknowledgments

The present study has been partially sponsored by CIUNSA and CONICET Projects.

Appendix A

The elements of the matrices $[Op^{(1)}]$ and $[Op^{(2)}]$ are given by:

$$[Op^{(1)}]=\begin{bmatrix} a'_1 & a'_2 & -a'_3 \\ b'_1 & b'_2 & -b'_3 \\ -c'_1 & -'_2 & c'_3 \end{bmatrix}$$

$$[Op^{(2)}]=\begin{bmatrix} \sum_{i=1}^{3} a'_i\alpha'_i & \sum_{i=1}^{3} a'_i\beta'_i \\ \sum_{i=1}^{3} b'_i\alpha'_i & \sum_{i=1}^{3} b'_i\beta'_i \\ -\sum_{i=1}^{3} c'_i\alpha'_i & -\sum_{i=1}^{3} c'_i\beta'_i \end{bmatrix}$$

where:

$$a'_1=\frac{J_{22}^2}{|\mathbf{J}|^2},\quad a'_2=\frac{J_{12}^2}{|\mathbf{J}|^2},\quad a'_3=2\frac{J_{12}J_{22}}{|\mathbf{J}|^2}$$

$$b'_1=\frac{J_{21}^2}{|\mathbf{J}|^2},\quad b'_2=\frac{J_{11}^2}{|\mathbf{J}|^2},\quad b'_3=2\frac{J_{11}J_{21}}{|\mathbf{J}|^2}$$

$$c'_1=\frac{J_{21}J_{22}}{|\mathbf{J}|^2},\quad c'_2=\frac{J_{11}J_{12}}{|\mathbf{J}|^2},\quad c'_3=\frac{J_{11}J_{22}+J_{12}J_{21}}{|\mathbf{J}|^2}$$

$$\alpha'_1=\frac{-J_{11,\xi}J_{22}+J_{12,\xi}J_{21}}{|\mathbf{J}|}\quad \alpha'_2=\frac{-J_{21,\eta}J_{22}+J_{22,\eta}J_{21}}{|\mathbf{J}|},$$

$$\alpha'_3=\frac{J_{11,\eta}J_{22}-J_{22,\xi}J_{21}}{|\mathbf{J}|}$$

$$\beta'_1=\frac{J_{11,\xi}J_{12}-J_{12,\xi}J_{11}}{|\mathbf{J}|},\quad \beta'_2=\frac{J_{21,\eta}J_{12}-J_{22,\eta}J_{11}}{|\mathbf{J}|},$$

$$\beta'_3=\frac{-J_{11,\eta}J_{12}+J_{22,\xi}J_{11}}{|\mathbf{J}|}$$

Appendix B

The first members $p_1^{(\bullet)}(\xi)$ $((\bullet)=w,\ \phi_x,\ \phi_y)$ for the different boundary conditions are:

Clamped–Clamped	Simply supported–Simply supported	Free–Free
$p_1^{(w)}(\xi)=1-2\xi^2+\xi^4$	$p_1^{(w)}(\xi)=-1+\xi^2$	$p_1^{(w)}(\xi)=1$
$p_1^{(\phi_x)}(\xi)=-1+\xi^2$	$p_1^{(\phi_x)}(\xi)=1$	$p_1^{(\phi_x)}(\xi)=1$
$p_1^{(\phi_y)}(\xi)=-1+\xi^2$	$p_1^{(\phi_y)}(\xi)=-1+\xi^2$	$p_1^{(\phi_y)}(\xi)=1$
Clamped–Simply supported	Clamped–Free	Simply supported–Free
$p_1^{(w)}(\xi)=-1-\xi+\xi^2+\xi^3$	$p_1^{(w)}(\xi)=1+2\xi+\xi^2$	$p_1^{(w)}(\xi)=1+\xi$
$p_1^{(\phi_x)}(\xi)=1+\xi$	$p_1^{(\phi_x)}(\xi)=1+\xi$	$p_1^{(\phi_x)}(\xi)=1+\xi$
$p_1^{(\phi_y)}(\xi)=-1+\xi^2$	$p_1^{(\phi_y)}(\xi)=1+\xi$	$p_1^{(\phi_y)}(\xi)=1$

References

[1] Reissner E. The effect of transverse shear deformation on the bending of elastic plate. Am Soc Mech Eng J Appl Mech 1945;12:69–76.
[2] Mindlin RD. Influence rotatory inertia and shear in flexural motion of isotropic, elastic plates. ASME J Appl Mech 1951;18:31–8.
[3] Pai PF. A new look at shear correction factors and warping functions of anisotropic laminates. Int J Solids Struct 1995;32(16):2295–313.
[4] Murthy MVV. An improved transverse shear deformation theory for laminated anisotropic plates. NASA Technical Paper; 1981.
[5] Reddy JN. A simple higher order shear deformation theory for laminated composite plates. J Appl Mech 1984;51(4):745–53.
[6] Bhimaradi A, Stevens LK. A higher order theory for free vibration of orthotropic, homogenous and laminated rectangular plates. J Appl Mech 1984;51:195–8.
[7] Pervez T, Seibi AC, Al-Jahwari FKS. Analysis of thick orthotropic composite plates based on higher order shear deformation theory. Compos Strcut 2005;71:414–22.
[8] Kant T, Swaminathan K. Analytical solution for the static analysis of laminated composite and sandwich based on higher order refined theory. Compos Struct 2002;56:329–44.
[9] Aydogdu M. Vibration analysis of cross-ply laminated beams with general boundary conditions by Ritz method. Int J Mech Sci 2005;47(11):1740–55.
[10] Shi G. A new simple third-order shear deformation theory of plates. Int J Solids Struct 2007;44:4399–417.
[11] Touratier M. An efficient standard plate theory. Int J Eng Sci 1991;29(8):745–52.
[12] Soldatos KP. A transverse shear deformation theory for homogenous monoclinic plates. Acta Mech 1992;94:195–220.
[13] Karama M, Afaq KS, Mistou S. Mechanical behavior of laminated composite beam by the new multilayered laminated composite structures model with transverse shear stress continuity. Int J Solids Struct 2003;40:1525–46.
[14] Karama M, Afaq KS, Mistou S. A new theory for laminated composite plates. Proc IMechE Part L: J Mater Des Appl 2009;223:53–62.
[15] Sahoo R, Singh BN. A new shear deformation theory for the static analysis of laminated composite and sandwich plates. Int J Mech Sci 2013;75:324–36.
[16] Mantari JL, Oktem AS, Soares CG. Static and dynamic analysis of laminated composite and sandwich plates and shells by using a new higher-order shear deformation theory. Compos Struct 2011;94:37–49.
[17] Mantari JL, Oktem AS, Soares CG. A new higher order shear deformation theory for sandwich and composite laminated plates. Compos Part B 2012;43:1489–99.
[18] Mantari JL, Oktem AS, Soares CG. A new trigonometric shear deformation theory for isotropic, laminated composite and sandwich plates. Int J Solids Struct 2012;49:43–53.
[19] Pradhan KK, Chakraverty S. Transverse vibration of isotropic thick rectangular plates based on new inverse trigonometric shear deformation theories. Int J Mech Sci 2015;94–95:211–31.
[20] Grover N, Singh BN, Maiti DK. Analytical and finite element modeling of laminated composite and sandwich plates: An assessment of a new shear deformation theory for free vibration response. Int J Mech Sci 2013;67:89–99.
[21] Thai CH, Ferreira AJM, Bordas SPA, Rabczuk T, Nguyen-Xuan H. Isogeometric analysis of laminated composite and sandwich plates using a new inverse trigonometric shear deformation theory. Eur J Mech A/Solids 2014;43:89–108.
[22] Carrera E. Historical review of zig-zag theories for multilayered plates and shells. Appl Mech Rev 2003;56:287–308.
[23] Reddy JN, Arciniega RA. Shear deformation plate and shell theories: from Stavsky to present. Mech Adv Mater Struct 2004;11:535–82.
[24] Wanji C, Zhen W. A selective review on recent development of displacement-based laminated plate theories. Recent Pat Mech Eng 2008;1:29–44.
[25] Liu L, Chua LP, Ghista DN. Mesh-free radial basis function method for static, free vibration and buckling analysis of shear deformable composite laminates. Compos Struct 2007;78:58–69.
[26] Kant T, Swaminathan K. Analytical solutions for free vibration of laminated composite and sandwich plates based on a higher-order refined theory. Compos Struct 2001;53(1):73–85.
[27] Xiang S, Wang KM. Free vibration analysis of symmetric laminated composite plates by trigonometric shear deformation theory and inverse multiquadric RBF. Thin Walled Strcut 2009;47:304–10.
[28] Ferreira AJM, Roque CMC, Martins PALS. Radial basis functions and higher-order shear deformation theories in the analysis of laminated composite beams and plates. Compos Struct 2004;66:287–93.
[29] Ferreira AJM, Roque CMC, Carrera E, Cinefra M. Analysis of thick isotropic and cross-ply laminated plates by radial basis functions and a Unified Formulation. J Sound Vib 2011;330:771–87.
[30] Reddy JN. Mechanics of laminated composite plates and shells – theory and analysis. Boca Raton: CRC Press; 2004.
[31] Dai KY, Liu GR, Lim KM, Chen XL. A mesh-free method for static and free vibration analysis of shear deformable laminated composite plates. J Sound Vib 2004;269(3–5):633–52.
[32] Carrera E. A class of two-dimensional theories for anisotropic multilayered plates analysis. Atti Accademia delle Scienze di Torino 1995;19-20:49–87.
[33] Dozio L, Carrera E. Ritz analysis of vibrating rectangular and skew multilayered plates based on advanced variable-kinematic models. Compos Struct 2012;94:2118–28.
[34] Ye T, Jin G, Su Z, Chen Y. A modified Fourier solution for vibration analysis of moderately thick laminated plates with general boundary restraints and internal line supports. Int J Mech Sci 2014;80:29–46.
[35] Jin G, Su Z, Shi S, Ye T, Gao S. Three-dimensional exact solution for the free vibration of arbitrarily thick functionally graded rectangular plates with general boundary conditions. Compos Struct 2014;108:565–77.
[36] Jin G, Ye T, Jia X, Gao S. A general Fourier solution for the vibration analysis of composite laminated structure elements of revolution with general elastic restraints. Compos Struct 2014;109:150–68.
[37] Jin G, Ye T, Ma X, Chen Y, Su Z, Xie X. A unified approach for the vibration analysis of moderately thick composite laminated cylindrical shells with arbitrary boundary conditions. Int J Mech Sci 2013;75:357–76.
[38] Jin G, Su Z, Ye T, Jia X. Three-dimensional vibration analysis of isotropic and orthotropic conical shells with elastic boundary restraints. Int J Mechanical Sci 2014;89:207–21.
[39] Su Z, Jin G, Shi S, Ye T, Jia X. A unified solution for vibration analysis of functionally graded cylindrical, conical shells and annular plates with general boundary conditions. Int J Mech Sci 2014;80:62–80.
[40] Jin G, Ye T, Chen Y, Su Z, Yan Y. An exact solution for the free vibration analysis of laminated composite cylindrical shells with general elastic boundary conditions. Compos Struct 2013;106:114–27.
[41] Ye T, Jin G, Chen Y, Ma X, Su Z. Free vibration analysis of laminated composite shallow shells with general elastic boundaries. Compos Struct 2013;106:470–90.
[42] Nallim LG, Oller S, Grossi RO. Statical and dynamical behaviour of thin fibre reinforced composite laminates with different shapes. Comput Methods Appl Mech Eng 2005;194:1797–822.

[43] Nallim LG, Oller S. An analytical-numerical approach to simulate the dynamic behaviour of arbitrarily laminated composite plate. Compos Struct 2008;85:311–25.
[44] Rektorys K. Variational methods in mathematics, science and engineering. Dordrecht: Reidel Co.; 1980.
[45] Arya H, Shimpi RP, Naik NK. A zigzag model for laminated composite beams. Compos Struct 2002;56:21–4.
[46] Ferreira AJM, Roque CMC, Jorge RMN. Analysis of composite plates by trigonometric shear deformation theory and multiquadrics. Comput Struct 2005;83(27):2225–37.
[47] Zienkiewicz OC, Taylor RL. sixth ed.The finite element method for solid and structural mechanics, Volume 2. . Great Britain: Elsevier; 2005.
[48] Rango RF, Nallim LG, Oller S. Static and dynamic analysis of thick laminated plates using enriched macroelements. Compos Struct 2013;101:94–103.
[49] Rango RF, Nallim LG, Oller S. Formulation of enriched macro elements using trigonometric shear deformation theory for free vibration analysis of symmetric laminated composite plate assemblies. Compos Struct 2015;119:38–49.
[50] Bhat RB. Plate deflection using orthogonal polynomials. J Eng Mech ASCE 1985;101:1301–9.
[51] Bhat RB. Natural frequencies of rectangular plates using characteristic orthogonal polynomials in Rayleigh–Ritz method. J Sound Vib 1985;102:493–9.
[52] Nallim LG, Grossi RO. On the use of orthogonal polynomials in the study of anisotropic plates. J Sound Vib 2003;264(5):1201–7.
[53] Reddy JN. Mechanics of laminated anisotropic plates: theory and analysis. Boca Raton, Florida: CRC Press; 1997.
[54] Shi JW, Nakatani A, Kitagawa H. Vibration analysis of fully clamped arbitrarily laminated plate. Compos Struct 2004;63(1):115–22.
[55] Liew KM. Solving the vibration of thick symmetric laminates by reissner/mindlin plate theory and thep-Ritz method. J Sound Vib 1996;198(3,5):343–60.
[56] Akhras G, Li W. Static and free vibration analysis of composite plates using spline finite strips with higher-order shear deformation. Compos Part B: Eng 2005;36(6–7):496–503.
[57] Eftekhari SA, Jafari AA. Modified mixed Ritz-DQ formulation for free vibration of thick rectangular and skew plates with general boundary conditions. Appl Math Model 2013;37(12–3):7398–426.